RSC Advances

ROYAL SOCIETY OF CHEMISTRY

PAPER

View Article Online
View Journal | View Issue

Check for updates

Cite this: *RSC Adv.*, 2024, **14**, 40133

Beryllium carbonate: a model compound for highest capacity carbon sequestration chemistry†

Gad Licht,[a] Kyle Hofstetter[b] and Stuart Licht *[abc]

Received 30th October 2024
Accepted 16th December 2024

DOI: 10.1039/d4ra07753a

rsc.li/rsc-advances

Beryllium carbonate has the highest capacity to bind and release the greenhouse gas CO_2 compared to amines, ionic liquids, $CaCO_3$ or Li_2CO_3. The thermodynamic equilibrium for CO_2 and BeO from $BeCO_3$ is calculated. TGA of $BeCO_3$ is used to determine the stepwise mechanism of its CO_2 release, and the low melting point $Li/Sr/BeCO_3$ is demonstrated.

Introduction

Rising CO_2 levels are causing catastrophic climate change, and are an existential threat to the planet. Atmospheric CO_2 levels, stable at 235 ($\pm$50) ppm for several hundred thousand years prior to the industrial revolution, have nearly doubled to 424 ppm and continue to rise rapidly. The effects of climate change include an increasing probability of a mass species extinction event.[1] The ongoing toll on humanity and the planet's habitats are increasingly evident; on a personal note, the first and third authors of this study have just experienced ground zero of two "once in a millennium rainfall events" (Hurricanes Helene and Milton) in a period of two weeks, while the middle author is subject to increasingly frequent forest fires.

A principal path to mitigate climate change is CO_2 sequestration, and CO_2 capture capacity is a measure of the extent of a chemical species binding of CO_2 for use in carbon sequestration chemistry. CO_2 capture capacity is quantified as mass or mole capacity of CO_2 per mass or mole of absorbent. In addition to the general need for effective CO_2 trapping materials to mitigate CO_2-induced global warming and climate change, other examples of the need for lightest weight carbon capture materials for CO_2 air scrubbing, include those needed by submersibles, submarines, and spacecraft.[2,3]

Several recent reviews have focused on amines (and amino acids), calcium oxide (to calcium carbonate), and ionic liquids to bind and release CO_2.[4–9] More recently, there has been a growing focus on nanomaterials, such as carbon nanomaterials,[10–12] and also on and lithium carbonate and mixed lithium/strontium carbonates[13–16] to capture CO_2 has emerged. Table 1 summarizes common absorbents including amines, ionic liquids, calcium oxide (to calcium carbonate), and more recently, lithium oxide (to lithium carbonate). In this study, beryllium carbonate is introduced as a model compound, establishing a baseline for among the highest capacities of CO_2 captured.

CO_2 can be captured and stored by thermal cycling. In this case, dilute CO_2 is generally introduced at a lower temperature and released in a concentrated form at a higher temperature. Thermal cycling can comprise adsorption chemistry, as generally occurs with various amine carbon capture chemistries,[5,7] or by chemical reactions, as occurs in the reaction of dissolved or solid calcium oxide with CO_2 to calcium carbonate, followed by high-temperature decomposition of calcium carbonate back to calcium oxide.[8] Thermal cycling is often accompanied by pressurization and also by different subsequent processes to sequester (Carbon Capture and Storage, CCS) or chemically convert (Carbon Capture Utilization and Storage, CCUS) the captured concentrated CO_2. As an alternative to thermal cycling, the CO_2 capture can be accomplished by electrolysis (such as the electrochemical splitting of CO_2 to C and O_2) to a product containing the captured CO_2, such as the formation of Carbon NanoTubes (CNTs) from CO_2 in molten carbonates.[17–20] This latter CCUS process often occurs in a single step.

In Table 1, the capacity for CO_2 is compiled for common CO_2 absorbents (absorbents referring to both adsorbents, absorbents, and reactants). The capacity for CO_2 is presented in units of both mole CO_2/mole absorbent and also in more typical units of kg CO_2 captured per kg absorbent in the last column. Pragmatic capacities for CO_2 will be lower than those compiled when a matrix (such as an inert membrane or solvent stabilizer) is required as an additional mass component in the CO_2 capture process.

Amines and amino acids have been widely studied both as absorbents, principally in the liquid phase, to absorb and release CO_2, and as adsorbents principally affixed on membranes to adsorb and release CO_2. As seen in Table 1, amines and amino acids have respective capacities for CO_2 of 0.19–0.37 or 0.27–0.35 kg CO_2 per kg (amine or amino acid). Ionic liquids have attained capacities of 0.07–0.09 kg CO_2 per kg. $CaO/CaCO_3$ has a capacity for CO_2 of 0.78 kg CO_2 (determined as of $CaO + CO_2 \rightarrow CaCO_3$

[a]C2CNT LLC, A4 188 Triple Diamond Blvd, North Venice, FL 34275, USA. E-mail: slicht@gwu.edu

[b]Carbon Corp, 1035 26 St NE, Calgary, AB T2A 6K8, Canada

[c]Dept. of Chemistry, George Washington University, Washington DC 20052, USA

† Electronic supplementary information (ESI) available. See DOI: https://doi.org/10.1039/d4ra07753a

Table 1 The high capacity for CO_2 of beryllium oxide as beryllium carbonate compared to other absorbents

Chemical absorbent/product	Acronym	Formula	Formula weight, g mol^{-1}	CO_2 storage mechanism	Capacity for CO_2, mol CO_2/mol absorbent	Source, reference	Capacity for CO_2, kg CO_2 per kg absorbent
1-Butyl-3-methylimidazolium bis(trifluoromethylsulfonyl) imide	[Bmim] [Tf_2N]	$C_{10}H_{15}F_6N_3O_4S_2$	419.37	Ionic liquid	0.68	7	0.07
1-Aminopropyl-3-methylimidazolium tetraborafluorate/various products	APMim [BF_4]	$C_7H_{14}N_3BF_4$	227.01	Ionic liquid	0.34	7	0.07
1-Butyl-3-methylimidazolium hexafluorophosphate/various products	[Bmim] [PF_6]	$C_8H_{15}F_6N_2P$	284.186	Ionic liquid	0.51	7	0.08
1-Butyl-3-methylimidazolium tetrafluoroborate/various products	[Bmim] [BF_4]	$C_8H_{15}BF_4N_2$	226.03	Ionic liquid	0.44	7	0.09
Taurine to protonated acid, HCO_3^- or carbamate		$C_2H_7NO_3S$	125.14	Amino acid	0.7	7	0.25
Proline to protonated acid, HCO_3^- or carbamate		$C_5H_9NO_2$	115.132	Amino acid	0.7	7	0.27
Glycine to protonated acid, HCO_3^- or carbamate		$C_2H_5NO_2$	75.067	Amino acid	0.6	7	0.35
Monoethanolamine to $RNHCOO^-$	MEA	$C_5H_{13}NO_2$	61.08	Amine	0.5	7	0.36
Diethanolamine to $RNHCOO^-$	DEA	$C_4H_{11}NO_2$	105.14	Amine	0.5	7	0.21
Methyldiethanolamine to ‘’	MDEA	$C_5H_{13}NO_2$	119.164	Amine	1	7	0.37
Diethylethanolamine to “”	DEAE	$C_6H_{15}NO$	117.192	Amine	0.5	7	0.19
Calcium oxide to carbonate		CaO	56.08	$CaO + CO_2 \rightarrow CaCO_3$	1	9	0.78
Lithium oxide to carbonate		Li_2O	29.88	$Li_2O + CO_2 \rightarrow Li_2CO_3$	1	16	1.47
Beryllium oxide to carbonate		BeO	24.01	$BeO + CO_2 \rightarrow BeCO_3$	1	This study	1.83

from the 44.01 g per mol FW of CO_2 to the 56.08 g per mol FW of CaO). The lighter molecular weight Li_2O/Li_2CO_3 has a capacity for CO_2 of 1.47 kg CO_2. In order of increasing CO_2 capacities, the absorbents are ionic liquids < amino acids & amines < CaO (to $CaCO_3$) < Li_2O (to Li_2CO_3).

In this study, beryllium carbonate, with the lowest melting points of inorganic carbonates, is introduced as a model compound establishing a baseline for maintaining the highest capacities for CO_2 (1.83 kg CO_2 per kg BeO → $BeCO_3$). Beryllium carbonate is also as an example of a melting point decrease facilitator by addition of $BeCO_3$ to binary Li/$SrCO_3$ electrolyte to become the substantially lower melting point ternary Li/Sr/$BeCO_3$. Binary mixtures typically melt at lower temperatures than pure components because the presence of different molecules disrupts the crystal lattice, weakening intermolecular forces and reducing the energy needed to melt, and in this case CO_2 release can then be achieved using a lower thermal energy input.

Results and discussion

Phase changes & CO_2 equilibria of alkali & alkali earth carbonates

As summarized in Table 2, the melting point of beryllium carbonate (mp 54 °C), Be_2CO_3, is low in the extreme compared to that of the other alkali earth or alkali carbonates, or compared to their binary or tertiary carbonate mixtures. It should be noted that reported values of carbonate melting points exhibit a considerable range of 10 °C or more. For example, in 7 studies, the melting point of Li_2CO_3 is reported from 700 °C to 728 °C.[22–28] Furthermore, the CO_2 concentration in the atmosphere has increased by 35% since the first of these reports appeared (in 1957). The stability of lithium carbonate increases under 1 atm of CO_2, and we also note that many properties, including melting points, of species related to CO_2 equilibrium will need to be reevaluated due to the rapidly increasing atmospheric concentration of this greenhouse gas.

Alkali carbonate binary mix eutectics have lower melting points. The lowest melting alkali carbonate is generally considered to be the $Li_xNa_yK_zCO_3$ with a melting point of 397 °C (at $\sim x = 0.47$, $y = 0.62$, $z = 0.5$), still considerably higher than the melting point of $BeCO_3$, by 343 °C.

The extent to which an alkali or alkali earth carbonates retains CO_2 is given by:

$$MCO_3 \rightleftharpoons CO_2(\text{gas}) + MO\ (M = Be, Mg, Li_2, Na_2, \textit{etc.}) \quad (1)$$

$$K = p_{CO_2}\, a_{MO}/a_{MCO_3};\ K(T) = e^{-\Delta G(T)/RT} \quad (2)$$

Table 2 Melting point of alkali and alkali earth carbonates and their eutectic mixtures

Carbonate	Melting point (°C)	Decomposition point (°C)	Ref.
Be_2CO_3	54	~100	21
Li_2CO_3, Na_2CO_3 or K_2CO_3	723, 851 or 891	~1300[a] (Li_2CO_3)	30
$BaCO_3$	810	~1360	31 and 32
$MgCO_3$	—	~350	32
$CaCO_3$	—	~850	31 and 32
$SrCO_3$	1494	1494	13
$Li_2/BaCO_3$; 55/45 mol%	609		31 and 34
$K_2CO_3/MgCO_3$; 57/43 mol%	460		35
Li_2/K_2CO_3; 62/38 mol%	498		35
Na_2/K_2CO_3; 56/44 mol%	710		35
$Li_2/Na_2/K_2CO_3$; 43.5/31.5/25 mol%	397		35
Li_2/Sr_2CO_3; 60/40 wt%	680		13
$Be/Sr/Li_2CO_3$; 33/33/33 wt%	480		This study

[a] Li_2CO_3 decomposition is more rapid under argon than under air.[15]

An extensive literature search did not reveal phase diagrams or equilibria for beryllium carbonate. We've calculated the $BeCO_3/BeO + CO_2$ equilibrium from the available enthalpy and entropy of the constituent species.[29]

Fig. 1 presents a comparison of the carbonate/oxide equilibrium constant for binding and releasing of CO_2 by beryllium carbonate compared to those for alkali, or other alkali earth carbonates as a function of temperature. Below any of the Fig. 1 equilibrium presented curves, that is, in the high CO_2 activity domain, the carbonate salt will spontaneously form from CO_2 and the salt's oxide. Above any Fig. 1 equilibrium curve, the low CO_2 activity domain ($a_{CO_2}\, a_{oxide}/a_{carbonate} < K$), the carbonate salt will spontaneously decompose. For example, as noted in Table 2, solid $MgCO_3$ decomposes at 350 °C, releasing bound CO_2, and as seen is the second largest (other than $BeCO_3$) of the eqn

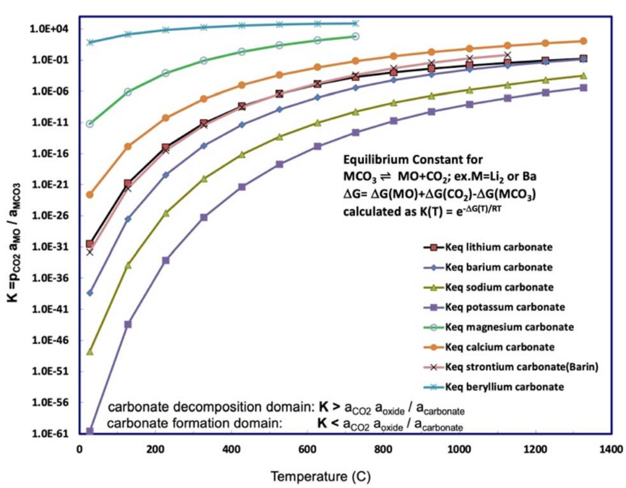

Fig. 1 Equilibrium constant for CO_2 release calculated for beryllium carbonate and compared to a range of alkali and alkali earth carbonates. The equilibrium constants as a function of temperature for strontium, lithium, sodium, potassium, and barium carbonate. The equilibrium constants are calculated from the free energy according to eqn (5). The free energy is calculated from the metal carbonate, metal oxide, and carbon dioxide enthalpies and entropies.[29,36–39]

(2) carbonate/oxide equilibrium constants. The high industrial carbon footprint conversion process of limestone to lime or cement depends on the solid state decomposition of calcium carbonate, such as aragonite, which occurs at ~850°.

Li_2CO_3/Li_2O was introduced as among the highest CO_2-capture materials, as delineated in the next to last row of Table 1, with a storage capacity of 1.47 kg CO_2 per kg Li_2O. Under argon, Li_2CO_3 entirely dissociates to $CO_2 + Li_2O$. Specifically, at a TGA rate of 5° min^{-1} under 1 atm of argon Li_2CO_3 dissociation starts around the lithium carbonate melting point of 723 °C, and is 98% complete to Li_2O by 900 °C, and under 1 atm of pure CO_2 also starts at 723 °C, but the dissociation is less than 10% complete by 900 °C.[15] However, under even small partial pressures of CO_2, such as the 426 ppm (and rising) of atmospheric CO_2, Li_2CO_3 only fractionally dissociates to CO_2, attaining 0.3 molal concentration Li_2O per kg molten Li_2CO_3 at 750 °C.[36] This high capacity was experimentally realized in the form of the electrolytic splitting of CO_2 in molten Li_2CO_3 to graphene nanocarbons.[40–49] The small concentration of dissolved Li_2O in molten Li_2CO_3 under air is sufficient to support high CO_2 splitting electrochemical current and continuous renewal of the molten Li_2CO_3 electrolyte with CO_2.[50]

The relationship between melting and decomposition temperatures for carbonates is complex. Beryllium carbonate has respective melting and decomposition points of $BeCO_3$ (M_p = 54 °C and D_p = 100 °C),[21] lithium carbonate Li_2CO_3 (M_p = 723 °C and D_p = 1300 °C), while as seen in Table 2, solid calcium and barium carbonate do not melt nor sublime, but rather decompose directly to calcium or barium oxide and carbon dioxide, finally, strontium carbonate has equivalent, but very high melting and decomposition points $SrCO_3$ ($M_p = D_p$ = 1494 °C). For binary and ternary mixtures, all the higher melting point carbonates are observed to be highly soluble in lithium carbonate. For example, over 60 wt% $SrCO_3$ is miscible in 750 °C molten Li_2CO_3.[13]

The temperature at which individual carbonates do, or do not, melt is observable and reproducible to within a few degrees. However, the decomposition point is much less distinct, occurring over hundreds of degrees. For example, while the formal Li_2CO_3 decomposition point in Table 2 is ~1300, substantial decomposition has already occurred at 750 °C with release of CO_2 and the resultant Li_2O forming as a dissolved salt within the molten Li_2CO_3.[36] Hence, this study focuses on the more precise melting point, rather than the broad range of observable decomposition point temperatures.

Beryllium carbonate as an ultra-high CO_2 storage material

When modeled as a specific example of eqn (1), beryllium carbonate is a high-capacity carbon capture storage material. Carbon dioxide is stored in beryllium carbonate and is released in the reaction to CO_2 and beryllium oxide:

$$BeCO_3 \rightleftharpoons CO_2(\text{gas}) + BeO \tag{3}$$

In accord with eqn (3), $BeCO_3$ (FW 69.02 g mol^{-1}) stores 44.01 g mol^{-1} CO_2/BeO (FW 25.01 g mol^{-1}) = 1.83 kg CO_2 per kg BeO → $BeCO_3$, as included in Table 1. As seen in Fig. 1, beryllium carbonate provides the largest of the equilibrium constants to release CO_2 of any of the alkali earth or alkali carbonates, and will begin to release CO_2 near ambient temperatures. At room temperature, beryllium carbonate (solid $BeCO_3$) is often stored under a blanket of CO_2 gas to prevent its decomposition. Beryllium oxide is the lightest weight oxide (other than water), and lithium and beryllium oxide have among the highest carbon capture storage capacities (as moles CO_2 storable per kg oxide).

Thermodynamically, $BeCO_3$ is the carbonate best suited to initiate storage and release of CO_2 at low temperatures. $BeCO_3$ is less prevalent as a salt than calcium, lithium, or strontium carbonate. Be is only the 48th most abundant element in the earth's upper crust,[51] and it and its oxide, particularly in powder form, is carcinogenic. However, the storage of CO_2 by $BeCO_3$ serves as a model for among the highest carbon storage capacity materials and lowest mass CO_2 scrubbers.

The stepwise mechanism of beryllium carbonate CO_2 storage

Eqn (1) only provides a thermodynamic overview of a carbonate's capability to release CO_2. The individual steps in the process of the binding of CO_2 into beryllium carbonate are investigated here by ThermoGravimetric Analysis, TGA.

Fig. 2 presents the TGA results of beryllium carbonate conducted from 30 °C, with a 5 °C temperature increase per minute, and in atmospheres of either (1) 80% N_2/20% O_2 gas mix shown in the orange curve from 30 to 730 °C or (2) 100% N_2 shown in the blue curve from 30 °C to 1000 °C. In the figure, the downward trend in the mass is seen to start at approximately, the cited[21] 54 °C melting of $BeCO_3$. The equivalence of the curves with or without an atmosphere containing O_2 provides primary evidence that O_2 is neither evolved nor absorbed by beryllium carbonate during the TGA, and that species in equilibrium with O_2, including oxides, peroxides, and superoxides, those species are not participants in reactions related to the TGA temperature sweep.

In Fig. 2 above 54 °C, $BeCO_3$ rapidly evolves CO_2 upon melting (at increasing temperature, the release of CO_2 from

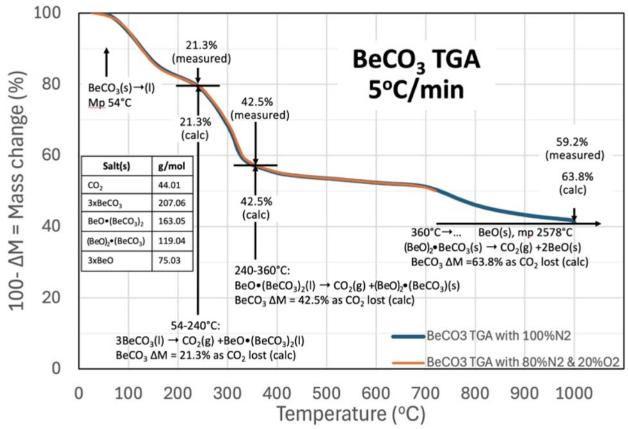

Fig. 2 TGA analysis of beryllium carbonate. The TGA is conducted from 30 °C with a 5 °C increase per minute in either (1) 80% N_2/20% O_2 (from 30 °C to 730 °C) or (2) 100% N_2 (from 30 °C to 1000 °C). Note, the observed TGA are identical (from 30 °C to 730 °C) in either the O_2 or pure N_2 environments.

$BeCO_3$ is an exergonic, spontaneous reaction). Released gases diffuse more slowly through a solid than through a liquid.[52] Salts evolving CO_2 from the liquid, as opposed to from the solid form, facilitate the rapid release of CO_2. For example, comparing liquid and solid CO_2 amine sorbents, solid gas reactions require much higher minimum work,[53] and the concurrent observed increased rate of mass loss acts as an indicator that the salt has melted. In solid salts that can release CO_2 by decomposition, CO_2 release is constrained by surface depletion and by the slow diffusion of CO_2 to the solid surface. Whereas, in the molten state, the liquid surface is continuously replenished, sustaining facile CO_2 access to the surface, and to the interior liquid bulk. In the figure, the mass loss and temperature are noted at the start of rapid mass declines with increasing temperature, and a mechanism of CO_2 mass loss is then determined by calculating mass consistent changes of the equivalent calcinated beryllium oxide and $BeCO_3$ salts.

As seen in Fig. 2, molten $BeCO_3$ evolves CO_2 to become $BeO\cdot(BeCO_3)_2$ from ~54 °C to 240 °C, consistent with the equivalence of both the observed and the calculated mass loss as mass loss (of CO_2/mass $BeCO_3$) of 21.3% when one CO_2 is evolved from 3 $BeCO_3$ to become $BeO\cdot(BeCO_3)_2$, and the rapid mass loss indicative of facile CO_2 evolution from a liquid. In the future, several orders of magnitude larger than the TGA mg size samples would be useful to visually corroborate that this is in the liquid (l) phase at these temperatures:

$$3BeCO_3(l) \rightarrow CO_2(g) + BeO\cdot(BeCO_3)_2(l) \; T = 54\text{–}240\ ^\circ C \tag{4}$$

At increasing temperature, the molten $BeO\cdot(BeCO_3)_2$ then evolves CO_2 to become $(BeO)_2\cdot BeCO_3$ (FW 119.04) from 240 °C to 360 °C; again, as determined by the equivalence of both the observed and the calculated mass loss of 42.5% when $2CO_2$ are evolved from $3BeCO_3$ to become $BeO\cdot(BeCO_3)$, and once again the rapid mass loss indicative of facile CO_2 evolution from a liquid:

$$BeO\cdot(BeCO_3)_2(l) \rightarrow CO_2(g) + (BeO)_2\cdot(BeCO_3)\ (s) \quad T = 240\text{–}360\ ^\circ C \tag{5}$$

From 360 °C to ~700 °C, there is an observed slow, steady rate of CO_2 evolution as the mass loss observed in Fig. 2 increases to 50.9% from the original $BeCO_3$. The slow rate of CO_2 evolution is evidence that the eqn (5) product may be solid, and the additional (50.9–42.5%) 8.4% mass loss from $3BeCO_3$ is evidence that the $2BeO\cdot(BeCO_3)$ has evolved an additional 0.4 CO_2 over this temperature range with either a lower thermodynamic drive to release CO_2, or has reverted to the solid phase.

$$(BeO)_2\cdot(BeCO_3)(s) \rightarrow 0.4CO_2(g) + (BeO)_{2.4}\cdot(BeCO_3)_{0.6}(l) \quad T = 360\text{–}700\ ^\circ C \tag{6a}$$

Equivalent to integral molecular values of:

$$5(BeO)_2\cdot(BeCO_3)(s) \rightarrow 2CO_2(g) + (BeO)_{12}(BeCO_3)_3(l) \quad T = 360\text{–}700\ ^\circ C \tag{6b}$$

Above 700 °C, the observed rate of mass loss and CO_2 evolution again increased, indicative that the product has once again entered a liquid phase as noted on the right side of eqn (6a). In eqn (6b) $(BeO)_{12}(BeCO_3)_3(l)$ is a generalization of the total equivalence of BeO and $BeCO_3$ in the product, and it is likely that this consists of a solid BeO (mp 2578 °C) in a liquid phase of mixed $BeO_x/BeCO_3$. This product then evolves CO_2 to become BeO(*s*) from ~700 °C onward. As the end product of the beryllium carbonate CO_2 loss is a solid, high melting point BeO (mp 2578 °C), and by 1000 °C, the mass observed mass loss has reached 59.2% of the full, calculated 63.8% CO_2 mass loss from $BeCO_3$. Holding the TGA temperature at 1000 °C for 4 more hours resulted in a further mass loss of 1.2% to 60.4% of the full, calculated 63.8% CO_2 mass loss from $BeCO_3$:

$$(BeO)_{2.4}\cdot(BeCO_3)_{0.6}(l) \rightarrow 3BeO(s);\ T = 700\ ^\circ C \text{ to } T > 1000\ ^\circ C \tag{7}$$

For an overall reaction of:

$$3BeCO_3(l) \rightarrow 3CO_2(g) + 3BeO;\ T = 54\ ^\circ C \text{ to } T > 1000\ ^\circ C \tag{8}$$

The thermal release of CO_2 from $BeCO_3$ does not result in the formation of powdered BeO, which can be toxic, but rather initially forms $BeO_y\cdot(BeCO_3)_y$, and then at highest levels of CO_2 release temperatures, forms BeO in the TGA as a sintered (solid) mass due to the high temperature of formation, rather than an easily dispersible and potentially toxic powder.

The kinetically and thermodynamic-driven release of CO_2 by heating $BeCO_3$ and beryllium oxide/carbonates intermediate compounds has been demonstrated, and will presumably similarly occur by alternatively reducing the pressure over those compounds, or by simultaneously heating and reducing the pressure of those compounds. Thermodynamically, the storage of CO_2 by beryllium oxide and beryllium oxide/carbonate intermediates is energetically favored by the reverse process of cooling or pressurizing under CO_2 beryllium oxide and beryllium oxide/carbonate intermediates and stores CO_2. Beryllium oxide is stable, and this stability to reaction can be overcome by introducing kinetic facilitation to increase the rate of CO_2 uptake by cooling and/or with pressurized CO_2.

Future studies can probe the likelihood that the reverse beryllium oxide reaction with CO_2 to beryllium carbonate can be facilitated by means including: (i) bubbling CO_2 through the various molten (liquid phase) stages of beryllium oxide and its beryllium oxide/carbonate intermediates or forming a liquid aerosol combined with CO_2, (ii) increasing the surface area of the various solid phases stages of beryllium oxide and its beryllium oxide/carbonate intermediates such as by forming a powder, solid aerosol or fixing it to a high surface membrane or aerogel while combining with CO_2, (iii) introducing the CO_2 by mixing with a combined solid and liquid phase (slush) of beryllium oxide/carbonate intermediates, (iv) or a multistep reaction to incorporate CO_2 into beryllium oxide such as, but not limited to, the (iva) the facile reaction of CO_2 with ammonium compounds to form ammonium carbonates and the (ivb) reaction of beryllium oxide with sulfate compounds to form beryllium sulfates, followed by the (ivc) the facile reaction of ammonium carbonates and beryllium sulfates to form $BeCO_3$.

Beryllium-induced carbonate electrolyte melting point decrease

Li_2CO_3 is expensive due its relative scarcity and due to its increasing demand as a primary resource for EVs, but is useful for CO_2 removal and its electrolytic transformation to graphene nanocarbons.[16] There is less demand for $SrCO_3$ and its derivative salts, such as SrO, are also much more abundant, and an order of magnitude less expensive than Li_2CO_3.[13,51] We had demonstrated that molten Li_2CO_3 based electrolytes are effective for CO_2 carbon capture by the electrolytic splitting of CO_2. Interestingly, we recently found that the replacement of the majority of the Li_2CO_3 by $SrCO_3$ and SrO is also effective. The low-Li_2CO_3 electrolytes based on $SrCO_3$ are substantially less expensive than comparable Li_2CO_3-based electrolytes, and are useful for splitting and transforming CO_2 to stable graphene nanocarbons including CNTs and carbon nano-onions (ESI†).[13] The use of an electrolyte that is a binary mixture (for example, Sr/Li carbonate or SrO/Li_2CO_3) that can provide a low melting point electrolyte that facilitates transition metal nucleated growth from CO_2 of nanographene carbon allotropes is preferred.[13,16,40,42,47] Low-Li_2CO_3 electrolysis may be performed using a planar, rather than a coiled, and brass, rather than Monel, cathode without substantially affecting low-lithium CNT growth from CO_2.[13,40,41]

Pure $SrCO_3$ has a high melting point of 1194 °C, and in accord with Table 2 does not decompose until temperatures ≫1000 °C. As previously noted and as measured by TGA, the rapid decomposition of pure Li_2CO_3 commences near the 723 °C melting under conditions of no CO_2 (argon) up through pure CO_2.[15] A binary $SrCO_3/Li_2CO_3$ mix has a melting point of 690–790 °C. The melting point increases as the weight percent of $SrCO_3$ in the binary mix increases from 40 to 65%. The eutectic containing 40 wt% $SrCO_3$ melts at 690 °C, while the binary 50% $SrCO_3$ mix melts at 695 °C (ESI†). Fig. 3 demonstrates that this binary mix melting point is substantially decreased by the inclusion of

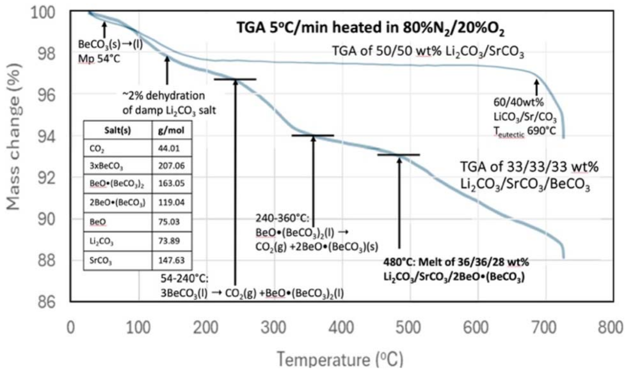

Fig. 3 TGA analysis of 50/50 wt% $Li_2CO_3/SrCO_3$ compared to 33.3/33.3/33.3 wt% $Li_2CO_3/SrCO_3/BeCO_3$. The TGA is conducted from 30 °C to 730 with a 5 °C increase per minute in 80% N_2/20% O_2.

$BeCO_3$ in a ternary mix. Specifically, Fig. 3 compares the TGA's of a binary mix 50/50 wt% $Li_2CO_3/SrCO_3$ to that of a ternary mix composed one-third by weight each in Li_2CO_3, $SrCO_3$, $BeCO_3$. The TGA starts from 30 °C, with a 5 °C min^{-1} temperature increase, and under an 80% N_2/20% O_2 gas mix.

For the TGA of the binary mix of 50/50 wt% $Li_2CO_3/SrCO_3$, a few percent weight loss is evident in Fig. 3 at low temperature as the damp material dries. Then the mass is moderately constant, decreasing slowly until a more rapid weight loss occurs around the 690 °C melting point observed for a $Li_2CO_3/SrCO_3$ mixture. Alternatively, in addition to the low-temperature drying, the 33.3/33.3/33.3 wt% $Li_2CO_3/SrCO_3/BeCO_3$ ternary mix exhibits the hallmarks of pure $BeCO_3$ up to a temperature of 360 °C that were seen in Fig. 2. However, in addition, another sharper decrease in mass loss is observed starting at 480 °C. These are attributed to the melting point of new lower melting ternary mixes of $Li_2CO_3/SrCO_3/BeO(BeCO_3)_2$ and specifically of 36/36/28 wt% $Li_2CO_3/SrCO_3/BeO$ when taking into account the loss of CO_2 up to 480 °C from the original $BeCO_3$ in the formation of BeO. Note, these wt% masses refer to the measured ratio of masses, as distributed through homogeneous speciation in the oxide dissolved in alkali earth carbonate melt, and not that there is a specific release of CO_2 from an isolated alkali earth carbonate within the liquid.

The melting point observed for the $Li_2CO_3/SrCO_3/BeCO_3$ ternary carbonate mix at 480 °C in Fig. 3 is 215 °C lower than the binary $Li_2CO_3/SrCO_3$mix without the beryllium carbonate addition. Hence, inclusion of $BeCO_3$ can lower the melting point of conventional inorganic carbonates prepared without a mix of $BeCO_3$.

Experimental

Thermodynamic carbonate/CO_2 equilibrium calculation

Enthalpies, entropies of species i, i = alkali and alkali earth carbonates, oxides, and CO_2 are from standard Barin, NIST (calculated from the available condensed phase thermochemistry data Shomate equations), and NASA data bases.[29–39] At any given temperature, the free energy of species "i" was calculated as:

$$\Delta G_i(T) = \Delta H_i(\mathrm{T}) - T\Delta S_i(T) \tag{9}$$

The free energy of equilibrium eqn (1) was then calculated as:

$$\Delta G_{\mathrm{eqn}\ (1)}(T) = \Delta G_{\mathrm{CO_2}}(T) + \Delta G_{\mathrm{MCO}}(T) - \Delta G_{\mathrm{MCO_3}}(T) \tag{10}$$

The eqn (1) equilibria constants for the various alkali and alkali earth carbonates were then calculated in accord with eqn (2).

TGA measurement, CO_2 evolution, and phase change

$BeCO_3$, 99+% purity, was from Chemsavers. Li_2CO_3 was purchased at a battery grade >99.5%, and used as received. The Li_2CO_3 had an analyzed composition of 99.8% (Li_2CO_3, Shanghai Seasongreen Chemical Co). The $SrCO_3$ used was 99.4% pure $SrCO_3$ (Shendong Zhi Chemical Co. Thermal) gravimetric analysis (TGA) was conducted using a PerkinElmer STA 6000 TGA/DSC TGA, under either pure N_2 or a mix of 80% N_2 and 20% O_2. TGAs were conducted with 15 mg of sample using a temperature ramp of 5 °C min^{-1} over the indicated temperature range. The daily reproducibility of known pure carbonate or graphene samples served as instrumental calibration, and any buildup of residual carbonate was removed by acid wash. In this study, the similarity of the measured mass change with or without the presence of O_2 was considered indicative that O_2 and related species were not participants in the mass loss sequence. TGA rapid mass loss was considered as gas evolved from the liquid phase, while a low rate of mass loss was considered an indicator of gas evolved from the solid phase as delineated in the text.

Conclusions

Rising levels of CO_2 in the atmosphere are driving catastrophic climate change, posing an existential threat to the planet. As CO_2 concentrations increase, they contribute to global warming, extreme weather events, and ecological disruptions. Addressing this challenge requires innovative solutions, one of which is CO_2 capture and sequestration.

The capacity for CO_2 is a crucial metric in assessing the effectiveness of various chemical species in absorbing, adsorbing or reacting CO_2 for sequestration purposes. This capacity is quantified as the amount of CO_2 (in kilograms) that can be captured per kilogram of the absorbent material. Common absorbents used in this field include amines, ionic liquids, and calcium oxide, which can transform into calcium carbonate. More recently, lithium oxide (Li_2O), which converts to lithium carbonate (Li_2CO_3), has gained attention as a potential absorbent.

In this study $BeCO_3$ has been introduced as a model compound due to its remarkably high CO_2 capture capacity. Although the practical application of beryllium is limited by its scarcity-ranking, as only the 48th most abundant element in the Earth's upper crust, it boasts a CO_2 capture capacity of 1.83 kg CO_2 per kg of BeO. This is significantly higher than that of other common absorbents: amines range from 0.19–0.37 kg CO_2 per kg, ionic liquids capture between 0.07 and 0.09 kg CO_2 per kg, calcium carbonate ($CaCO_3$) with a capacity of 0.78 kg CO_2 per kg, and lithium carbonate (Li_2CO_3) that captures 1.47 kg CO_2 per kg Li_2O.

To better understand the thermodynamics involved, the equilibrium between CO_2 and beryllium oxide (BeO) derived from $BeCO_3$ has been calculated and compared to various alkali and alkaline earth carbonates. Thermogravimetric analysis (TGA) of $BeCO_3$ has also been conducted to elucidate the stepwise mechanism of CO_2 release, providing insights into how this process in a stepwise release of CO_2 at increasing different temperatures.

Additionally, the influence of $BeCO_3$ on the melting point of mixtures has been explored. A comparison of the binary carbonate system consisting of Li_2CO_3 and strontium carbonate ($SrCO_3$) with a ternary system that includes $BeCO_3$ illustrates how the addition of $BeCO_3$ can substantially depress the melting point. $BeCO_3$ has been presented as a model carbonate to advance the foundation of understanding of the requirements of maximum carbon sequestration. It should be emphasized that beryllium, beryllium carbonate and beryllium oxide are more toxic, less abundant and therefore less available and more expensive than previously studied lower sequestration capacity lithium, magnesium and calcium compounds. This research not only highlights the unique properties of $BeCO_3$, but also contributes to the broader understanding of CO_2 capture technologies and their potential role in mitigating climate change.

Data availability

The data supporting this article have been included as part of the ESI.†

Author contributions

G. L. and S. L. designed the research; K. H., G. L. and S. L. performed the research and analysed the data; G. L. and S. L. wrote the paper.

Conflicts of interest

There are no conflicts to declare.

Acknowledgements

We are grateful to Emissions Reduction Alberta award IT0162473 for partial support of this research.

Notes and references

1 M. C. Urban, Accelerating extinction risk from climate change, *Science*, 2015, **348**, 571–573.
2 H. M. Baek, Possibility of service-regeneration of LiPH for submarines and improvements in CO_2 scrubbing performance in LiOH canisters, *JAMET*, 2022, **46**, 115–121.
3 S. Satayapal, T. Filburn, J. Trela and J. Strange, Performance and Properties of a Solid Amine Sorbent for Carbon Dioxide Removal in Space Life Support Applications, *Energy Fuels*, 2001, **15**, 250–255.
4 C. F. Martín, M. G. Plaza, J. J. Pis, F. Rubiera, C. Pevida and T. A. Centeno, On the limits of CO_2 capture capacity of carbons, *Sep. Purif. Technol.*, 2010, **74**, 225–229.
5 J. Y. Lai, L. H. Ngu and S. S. Hashim, A review of CO_2 adsorbents performance for different carbon capture technology processes conditions, *Greenhouse Gases:Sci. Technol.*, 2021, **11**, 1076–1117.
6 E. Victor, K. Chukwuemeka, O. A. Blessing, I. C. Success, O. Chisom, E. B. Chukwuemeka and N. U. Christian, A Concise Review of Sorbent Materials for Carbon Dioxide Capture and Storage, *J. Mat. Sci. Res. Rev.*, 2022, **10**, 72–98.
7 S. Y. W. Chai, L. H. Ngu and B. S. How, Review of carbon capture adsorbents for CO2 utilization, *Greenhouse Gases:Sci. Technol.*, 2022, **12**, 394–427.
8 Y. Tan, W. Liu, X. Zhang, W. Wei and S. Song, Conventional and optimized testing facilities of calcium looping process for CO_2 capture: A systematic review, *Fuel*, 2024, **358**, 130337.
9 S. Licht, Efficient solar-driven synthesis, carbon capture and desalinization, STEP, *Adv. Mater.*, 2011, **23**, 5592–5612.
10 M. Firdaus, A. Desforges, A. R. Mohamed and B. Vigolo, Progress in adsorption capacity of nanomaterials for carbon dioxide capture: A comparative study, *J. Cleaner Prod.*, 2021, **328**, 129553.
11 Y. Deng, J. Li, Y. Mia and D. Izikowitz, A comparative review of performance of nanomaterials for Direct Air Capture, *Energy Rep.*, 2021, **7**, 3506–3516.
12 X. Wang, T. He, J. Hu and M. Liu, The progress of nanomaterials for carbon dioxide capture *via* the adsorption process, *Environ. Sci.:Nano*, 2021, **8**, 890–912.
13 G. Licht, K. Hofstetter and S. Licht, A new electrolyte for molten carbonate decarbonization, *Commun. Chem.*, 2024, **7**, 211.
14 Q. Zhu, Y. Zeng and Y. Zheng, Overview of CO_2 capture and electrolysis technology in molten salts: operational parameters and their effects, *Ind. Chem. Mater.*, 2023, **1**, 59.
15 L. Shi, T. Qu, D. Liu, Y. Deng, B. Yang, and Y. Dai, Process of Thermal Decomposition of Lithium Carbonate, in *Materials Processing Fundamentals*, J., Lee, S., Wagstaff, G., Lambotte, A., Allanore and F., Tesfaye, The Minerals, Metals & Materials Series, 2020.
16 J. Ren, A. Yu, P. Peng, M. Lefler, F.-F. Li and S. Licht, Recent advances in solar thermal electrochemical process (STEP) for carbon neutral products and high value nanocarbons, *Acc. Chem. Res.*, 2019, **52**, 3177–3187.
17 J. Ren, F.-F. Li, J. Lau, L. Gonzalez-Urbina and S. Licht, One-pot synthesis of carbon nanofibers from CO_2, *Nano Lett.*, 2015, **15**, 6142–6148, DOI: **10.1021/jp9044644**.
18 J. Ren and S. Licht, Tracking airborne CO_2 mitigation and low cost transformation into valuable carbon nanotubes, *Sci. Rep.*, 2016, **6**, 27760, DOI: **10.1038/srep27760**.
19 G. Licht, K. Hofstetter and S. Licht, Polymer composites with carbon nanotubes made from CO_2, *RSC Sustainability*, 2024, **2**, 2496–2504.

20 G. Licht, K. Hofstetter and S. Licht, Buckypaper made with carbon nanotubes derived from CO_2, *RSC Adv.*, 2024, **14**, 27195–27197.
21 R. C. Ropp, *Encyclopedia of the Alkaline Earth Compounds*, Elsevier, Netherlands, pp. 359–360, 2013, ISBN 9780444595539.
22 *The Differential Thermal Investigations of Clays*, ed. T. L. Webb, H. Heystek and R. C. Mackenzie, Mineralogical Society, London, 1957, p.329.
23 A. D. Pelton, C. W. Bale and P. L. Lin, *Can. J. Chem.*, 1984, **62**, 457.
24 L. Barin, in *Thermochemical Data of Pure Substances*, VCH, Weinheim, 1989, pp.1–9.
25 N. N. Semenov, T. V. Zablotskii, I. Sib and O. Akad, *Nauk SSSR*, 1962, **2**, 58.
26 E. I. Maslova, I. S. Lileev, I. Sib and O. Akad, *Nauk SSSR*, 1958, **1**, 63.
27 L. S. Itkinaa and nd N. M. Chaplygina, *Russ. J. Inorg. Chem.*, 1962, **7**, 1456.
28 Y. Otsubo and K. Yamaguchi, *J. Chem.Soc.Japan*, 1961, **82**, 557.
29 M. Leader, curator, NASA Glenn ThermoBuild thermodynamic database,https://cearun.grc.nasa.gov/ThermoBuild/; last accessed April 17, 2024.
30 S. Licht, B. Wang, S. Ghosh, H. Ayub, D. Jiang and J. Ganley, A new solar carbon capture process: STEP carbon capture, *J. Phys. Chem. Lett.*, 2010, **1**, 2363–2368.
31 S. Licht and B. C. B. Wang, STEP carbon capture: the barium advantage, *J. CO_2 Util.*, 2013, **2**, 303–312.
32 X. Wang, G. Licht, X. Liu and S. Licht, CO_2 utilization by electrolytic splitting to carbon nanotubes in non-lithiated, cost effective, molten carbonate electrolytes, *Adv. Sustainable Syst.*, 2022, **2022**, 2100481.
33 J. Ren, M. Johnson, R. Singhal and S. Licht, Transformation of the greenhouse gas CO2 by molten electrolysis into a wide controlled selection of carbon nanotubes, *J. CO_2 Util.*, 2017, **18**, 335–344.
34 P. Pasierb, R. Gajerski, M. Rokita and M. Rekas, Studies on the binary system Li_2CO_3-$BaCO_3$, *Physica B*, 2001, **304**, 463–476.
35 S. Fangini and A. Masi, Molten carbonates for advanced and sustainable energy applications: Part 1, *Int. J. Hydrog. Energy*, 2016, **41**, 18739–19746.
36 J. Ren, J. Lau, M. Lefler and S. Licht, S. The minimum electrolytic energy needed to convert carbon dioxide to carbon by electrolysis in carbonate melts, *J. Phys. Chem. C*, 2015, **119**, 23342–23349.
37 P. J. Linstrom and G. Mallard, NIST Chemistry WebBook. NIST Standard Reference Database Number 69, 2001, National Institute of Standards and Technology, *J. Chem. Eng. Data*, 2001, **46**(5), 1059–1063.
38 J. Malcom and W. Chase, *NIST-JANAF Thermochemical Tables Fourth Ed. Amer Chem Soc*, Amer Inst Phys, Nat Inst Stand Tech, 1998, http://webbook.nist.gov, retrieved April 22, 2024.
39 L. Barin, *Thermochemical Data of Pure Substances. Part II*, VCH, 1989, pp. 1418–1427.
40 X. Liu, G. Licht and S. Licht, Controlled Transition Metal Nucleated Growth of Carbon Nanotubes by Molten Electrolysis of CO_2, *Catalysts*, 2022, **12**, 137.
41 X. Liu, G. Licht, X. Wang and S. Licht, Controlled Growth of Unusual Nanocarbon Allotropes by Molten Electrolysis of CO_2, *Catalysts*, 2022, **12**, 137.
42 X. Liu, G. Licht and S. Licht, The green synthesis of exceptional braided, helical carbon nanotubes and nanospiral platelets made directly from CO_2, *Mater. Today Chem.*, 2021, **22**, 100529.
43 X. Wang, G. Licht, X. Liu and S. Licht, One pot facile transformation of CO_2 to an unusual 3-D nan-scaffold morphology of carbon, *Sci. Rep.*, 2020, **10**, 21518.
44 X. Liu, J. Ren, G. Licht, X. Wang and S. Licht, Carbon nano-onions made directly from CO_2 by molten electrolysis for greenhouse gas mitigation, *Adv. Sustain. Syst.*, 2019, **3**, 1900056.
45 X. Liu, X. Wang, G. Licht and S. Licht, Transformation of the greenhouse gas carbon dioxide to graphene, *J. CO_2 Util.*, 2020, **236**, 288–294.
46 X. Wang, X. Liu, G. Licht and S. Licht, Calcium metaborate induced thin walled carbon nanotube syntheses from CO_2 by molten carbonate electrolysis, *Sci. Rep.*, 2020, **10**, 15146.
47 X. Wang, F. Sharif, X. Liu, G. Licht, M. Lefler and S. Licht, Magnetic carbon nanotubes: Carbide nucleated electrochemical growth of ferromagnetic CNTs, *J. CO_2 Util.*, 2020, **40**, 101218.
48 M. Johnson, J. Ren, M. Lefler, G. Licht, J. Vicini, X. Liu and S. Licht, Carbon nanotube wools made directly from CO_2 by molten electrolysis: Value driven pathways to carbon dioxide greenhouse gas mitigation, *Mater. Today Energy*, 2017, **5**, 230–236.
49 J. Ren, M. Johnson, R. Singhal and S. Licht, Transformation of the greenhouse gas CO_2 by molten electrolysis into a wide controlled selection of carbon nanotubes, *J. CO_2 Util.*, 2017, **18**, 335–344.
50 G. Licht, K. Hofstetter and S. Licht, Separation of Molten Electrolyte from the Graphene Nanocarbon Product Subsequent to Electrolytic CO_2 Capture, *Decarbon*, 2024, **4**, 100044.
51 Z. Hu and S. Gao, Upper crustal abundances of trace elements: A revision and update, *Chem. Geol.*, 2008, **253**, 205–221.
52 A. Kantzas, J. Bryan, S. Taheri, *Molecular Diffusion, Chapt. 3 in Fundamentals of Fluid Flow in Porous*, Media PERM, 2024, available at: https://perminc.com/resources/fundamentals-of-fluid-flow-in-porous-media/chapter-3-molecular-diffusion/.
53 H. S. Caram, R. Gupta, H. Thomann, F. Ni, S. C. Weston and M. Afeworki, A simple thermodynamic tool for assessing energy requirements for carbon capture using solid or liquid sorbents, *Int. J. Greenhouse Gas Control*, 2020, **97**, 102986.